Article

Cell Host & Microbe

An Asymmetric Opening of HIV-1 Envelope Mediates Antibody-Dependent Cellular Cytotoxicity

Graphical Abstract

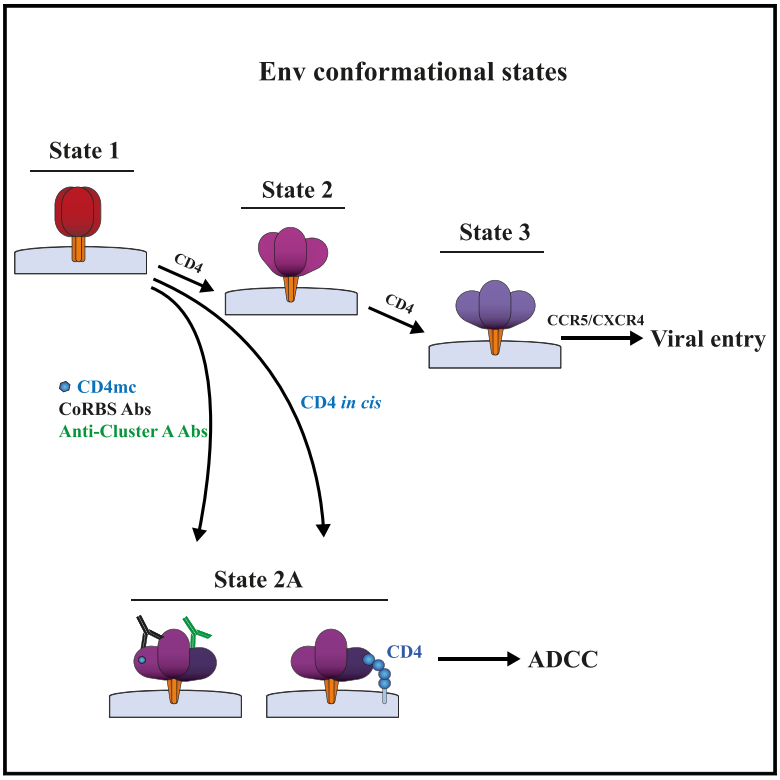

Highlights

- HIV Env exists in several conformations, including an asymmetric State 2A
- State 2A is difficult to trigger and is susceptible to non-neutralizing antibody attack
- Sera from HIV+ individuals contain antibodies that can stabilize Env State 2A
- Conditions triggering State 2A expose epitopes that induce ADCC

Authors

Nirmin Alsahafi, Nordine Bakouche, Mohsen Kazemi, ..., Isabelle Rouiller, Andrés Finzi, James B. Munro

Correspondence

isabelle.rouiller@unimelb.edu.au (I.R.), andres.finzi@umontreal.ca (A.F.), james.munro@tufts.edu (J.B.M.)

In Brief

HIV-1 envelope glycoproteins (Env) are very flexible and exist in at least three different conformational states. Alsahafi et al. characterize a fourth Env state that is efficiently recognized by antibodies capable of mediating potent antibody-dependent cellular toxicity.

Alsahafi et al., 2019, Cell Host & Microbe *25*, 578–587
April 10, 2019
https://doi.org/10.1016/j.chom.2019.03.002

CellPress

CellPress

Cell Host & Microbe
Article

An Asymmetric Opening of HIV-1 Envelope Mediates Antibody-Dependent Cellular Cytotoxicity

Nirmin Alsahafi,[1,2,15] Nordine Bakouche,[3,15] Mohsen Kazemi,[4,15] Jonathan Richard,[1,5] Shilei Ding,[1,5] Sudipta Bhattacharyya,[4] Durba Das,[4] Sai Priya Anand,[1,2] Jérémie Prévost,[1,5] William D. Tolbert,[6] Hong Lu,[7] Halima Medjahed,[1] Gabrielle Gendron-Lepage,[1] Gloria Gabrielle Ortega Delgado,[1] Sharon Kirk,[8] Bruno Melillo,[8] Walther Mothes,[9] Joseph Sodroski,[10,11,12] Amos B. Smith III,[8] Daniel E. Kaufmann,[1,5,13,14] Xueling Wu,[7] Marzena Pazgier,[6] Isabelle Rouiller,[4,15,*] Andrés Finzi,[1,2,5,15,*] and James B. Munro[3,15,16,*]

[1]Centre de Recherche du CHUM, Montreal, QC, Canada
[2]Department of Microbiology and Immunology, McGill University, Montreal, QC, Canada
[3]Department of Molecular Biology and Microbiology, Tufts University School of Medicine, Boston, MA, USA
[4]Department of Biochemistry and Molecular Biology and Bio21 Molecular Science and Biotechnology Institute, The University of Melbourne, Parkville, VIC, Australia
[5]Département de Microbiologie, Infectiologie et Immunologie, Université de Montréal, Montreal, QC, Canada
[6]Infectious Diseases Division, Uniformed Services University of the Health Sciences, Bethesda, MD, USA
[7]Aaron Diamond AIDS Research Center, Affiliate of The Rockefeller University, New York, NY, USA
[8]Department of Chemistry, School of Arts and Sciences, University of Pennsylvania, Philadelphia, PA 19104-6323, USA
[9]Department of Microbial Pathogenesis, Yale University School of Medicine, New Haven, CT 06536, USA
[10]Department of Cancer Immunology and Virology, Dana-Farber Cancer Institute, Boston, MA 02215, USA
[11]Department of Microbiology and Immunobiology, Harvard Medical School, Boston, MA 02115, USA
[12]Department of Immunology and Infectious Diseases, Harvard T.H. Chan School of Public Health, Boston, MA 02115, USA
[13]Department of Medicine, Université de Montréal, Montreal, QC, Canada
[14]Center for HIV/AIDS Vaccine Immunology and Immunogen Discovery, The Scripps Research Institute, La Jolla, CA 92037, USA
[15]These authors contributed equally
[16]Lead Contact
*Correspondence: isabelle.rouiller@unimelb.edu.au (I.R.), andres.finzi@umontreal.ca (A.F.), james.munro@tufts.edu (J.B.M.)
https://doi.org/10.1016/j.chom.2019.03.002

SUMMARY

The HIV-1 envelope glycoprotein (Env) $(gp120\text{-}gp41)_3$ is the target for neutralizing antibodies and antibody-dependent cellular cytotoxicity (ADCC). HIV-1 Env is flexible, sampling different conformational states. Before engaging CD4, Env adopts a closed conformation (State 1) that is largely antibody resistant. CD4 binding induces an intermediate state (State 2), followed by an open conformation (State 3) that is susceptible to engagement by antibodies that recognize otherwise occluded epitopes. We investigate conformational changes in Env that induce ADCC in the presence of a small-molecule CD4-mimetic compound (CD4mc). We uncover an asymmetric Env conformation (State 2A) recognized by antibodies targeting the conserved gp120 inner domain and mediating ADCC. Sera from HIV+ individuals contain these antibodies, which can stabilize Env State 2A in combination with CD4mc. Additionally, triggering State 2A on HIV-infected primary $CD4^+$ T cells exposes epitopes that induce ADCC. Strategies that induce this Env conformation may represent approaches to fight HIV-1 infection.

INTRODUCTION

Env resides on the surface of the HIV-1 virion, engages CD4 and a coreceptor, and promotes entry into the target cell. Single-molecule Förster resonance energy transfer (smFRET) imaging experiments directly demonstrated that Env is a highly dynamic molecule, which transitions from a "closed" conformation (State 1) to an "open" conformation that is recognized by CD4 (State 3). CD4 engagement induces an asymmetric intermediate (State 2) adopted on the pathway to State 3 (Herschhorn et al., 2016; Ma et al., 2018; Munro et al., 2014). Env also represents the only viral antigen exposed on the surface of virions and infected cells, and thus it is the primary target for antibodies (Abs). Env-targeting Abs can neutralize the virus or induce the death of infected cells through Ab-dependent cellular cytotoxicity (ADCC). Envs from primary HIV-1 isolates are relatively resistant to easily elicited CD4-induced (CD4i) Abs, which are predominant in HIV-1-infected individuals (Decker et al., 2005; Richard et al., 2018; von Bredow et al., 2016). This resistance is likely due to the stability of State 1 in primary Envs, which rarely make spontaneous transitions to conformations recognized by CD4 (Munro et al., 2014). CD4 engagement drives Env into States 2 and 3 and renders Env susceptible to CD4i Ab attack (Herschhorn et al., 2016; Madani et al., 2017; Prevost et al., 2017, 2018a; Veillette et al., 2014b, 2015).

Despite different mechanisms used by primary Envs to limit the spontaneous exposure of CD4i epitopes, the susceptibility

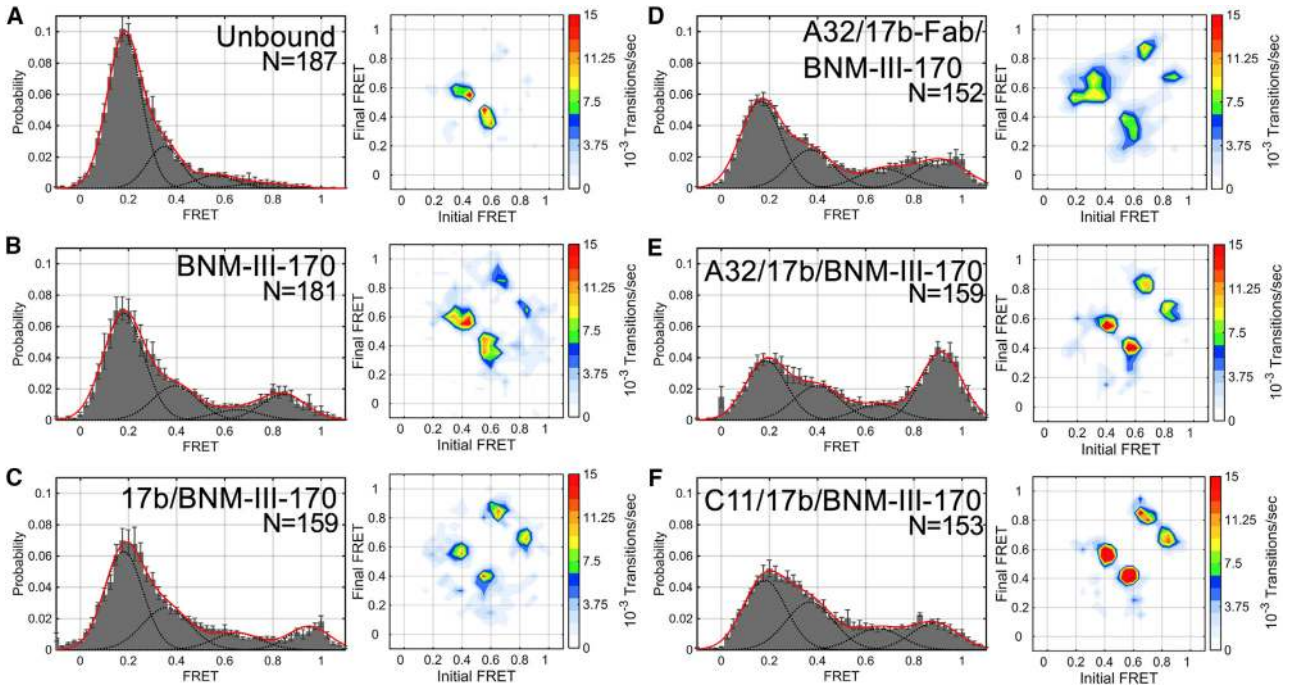

Figure 1. CD4mcs in Combination with Anti-cluster A and CoRBS Abs Stabilize Env State 2A

Histograms of FRET values (left) and TDPs resulting from HMM analysis (right) observed for HIV-1_{JR-FL} Env ΔCT (A) in the absence of bound ligands, and in the presence of (B) CD4mc BNM-III-170; (C) both BNM-III-170 and the CD4i Ab 17b; (D) BNM-III-170, 17b Fab, and the anti-cluster A Ab A32; (E) BNM-III-170, 17b, and A32; or (F) BNM-III-170, 17b, and C11. In all cases, the CD4mc was used at 100 μM, and Abs or Fab were used at 5 μg/mL. The FRET histograms were formed by compiling the indicated number (N) of smFRET traces. Overlaid on the histograms is the sum (red) of four Gaussian distributions with means and standard deviations determined by HMM analysis (0.18 ± 0.09, 0.38 ± 0.09, 0.65 ± 0.09, 0.90 ± 0.08; gray). Error bars reflect the standard deviation in the number of data points per histogram bin determined from three independent groups of smFRET traces.

of the cell to ADCC mediated by CD4i Abs dramatically increases when CD4 interacts with Env on the surface of infected cells (Veillette et al., 2014a, 2014b, 2015). Downregulation of cell-surface CD4 expression by the HIV-1 accessory proteins Nef and Vpu minimizes this effect (Alsahafi et al., 2016; Veillette et al., 2014b, 2015). Small CD4-mimetic compounds (CD4mcs) may promote conformational changes in Env similar to those observed upon CD4 binding (Melillo et al., 2016; Schon et al., 2006). This conformational change results in the sensitization of HIV-1-infected cells to ADCC mediated by CD4i Abs present in biological fluids, such as sera, breast milk, and cervicovaginal fluids (Richard et al., 2015, 2016, 2017). These small-molecule CD4mcs expose CD4i epitopes located in different Env elements such as the coreceptor binding site (CoRBS), the V1/V2 and V3 regions, and in gp41 (Gohain et al., 2016; Herschhorn et al., 2016; Madani et al., 2017; Melillo et al., 2016; Richard et al., 2016). However, only CD4i anti-cluster A Abs mediate potent ADCC (Ding et al., 2016; Richard et al., 2016). These Abs recognize the first and second (C1–C2) regions of the inner domain of gp120 in its CD4-bound conformation (Finzi et al., 2010; Guan et al., 2013). A32 and C11 are two prototypical Abs of this class and recognize distinct and non-overlapping epitopes within the cluster A region (Acharya et al., 2014; Tolbert et al., 2016, 2017). This region is buried inside the Env trimer and is not readily accessible when Env is in the State 1 conformation (Acharya et al., 2014; Ding et al., 2016; Tolbert et al., 2016; Veillette et al., 2014b; von Bredow et al., 2016). However, Env binding to CD4 at the cell surface readily exposes this region, enabling ADCC mediated by anti-cluster A Abs (Acharya et al., 2014; Alsahafi et al., 2016; Prevost et al., 2018b; Veillette et al., 2014b, 2015). Interestingly, while soluble CD4 (sCD4) or small-molecule CD4mcs can readily expose CD4i epitopes, they fail to expose cluster A epitopes on their own (Richard et al., 2016). A sequential opening of Env appears to be required to expose these epitopes. Indeed, it was shown that CD4mcs initially open the Env trimer allowing for CoRBS Abs engagement, which further opens the trimer, exposing cluster A epitopes (Richard et al., 2016). Binding of both CoRBS and cluster A Abs to Env efficiently engages FcγRIIIa and mediates robust ADCC (Anand et al., 2018).

Here, using a combination of smFRET imaging, Ab-binding and ADCC assays, and cryoelectron microscopy (cryo-EM), we have investigated the conformational dynamics required to expose cluster A epitopes in the presence of a small-molecule CD4mc. We report that Abs against this region stabilize an asymmetric Env conformation that was previously uncharacterized (State 2A). This conformation can be triggered with sCD4 or a CD4mc, a CoRBS Ab, and two different anti-cluster A Abs. Sera from HIV+ individuals also contain these Abs, which, in the presence of a CD4mc, trigger the transition of Env into State 2A. Finally, we show that the conditions that trigger State 2A also expose cluster A epitopes on the surface of primary $CD4^+$ T cells isolated from HIV-1-infected individuals.

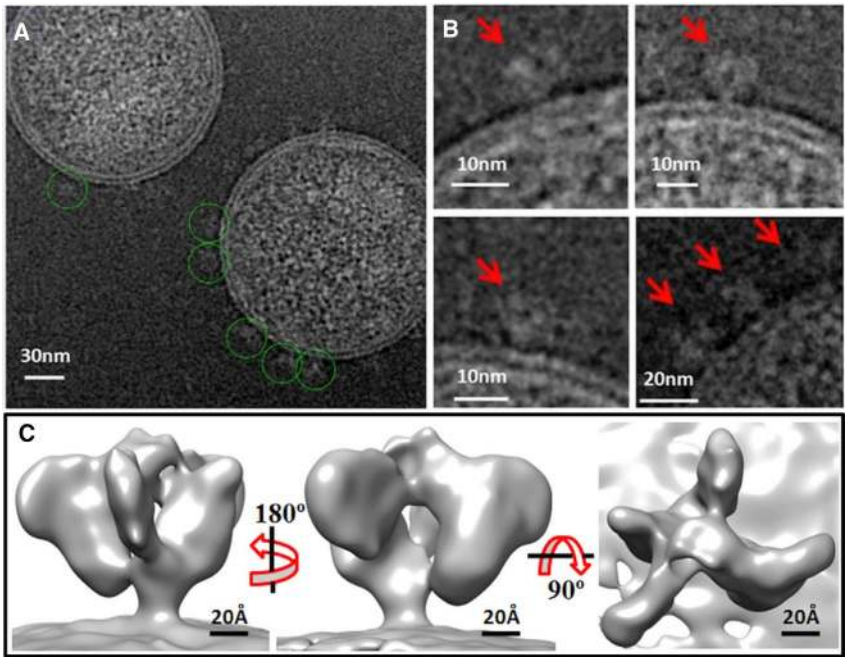

Figure 2. Cryo-EM Imaging of AT-2-Inactivated HIV-1 Particles with CD4mc BNM-III-170 in the Presence of 17b and A32 Antibodies

(A) AT-2-inactivated HIV-1 viral particles embedded in vitreous ice with spikes highlighted by green circles.

(B) Magnified images of single-membrane-bound spikes as indicated by red arrows. The images were collected with a K2 camera mounted on a Talos Arctica cryo-TEM. For improved visualization purposes, the images shown here were filtered using Gaussian blur with 2.0 sigma and contrast enhanced with 4% saturated pixels.

(C) Reconstructed ~13 Å cryo-EM map of the asymmetric HIV-1 Env in complex with the CD4mc (BNM-III-170) in the presence of the 17b- and A32-anti-HIV-1 antibodies.

RESULTS

Anti-cluster A Antibodies Recognize a Conformation that Differs from States 2 and 3

Binding of the CD4mc BNM-III-170 promotes conformational changes in Env similar to those observed upon CD4 binding (Lalonde et al., 2012; Schon et al., 2006). This triggers the exposure of several CD4i epitopes including the CoRBS and the V3 loop (Herschhorn et al., 2016; Lalonde et al., 2012; Madani et al., 2017; Schon et al., 2006), which is consistent with the stabilization of Env in States 2 and 3 (Herschhorn et al., 2016; Munro et al., 2014). Interestingly, despite exposing several CD4i epitopes, CD4mcs fail to expose those recognized by the anti-cluster A family of Abs (Richard et al., 2016) (Figures S1A and S1B). This suggests that anti-cluster A Abs recognize an Env conformation that differs from that recognized by anti-CoRBS and anti-V3 Abs. Addition of the 17b anti-CoRBS Abs (or its Fab′2, but not Fab, fragment) together with CD4mc was required to obtain efficient anti-cluster A Ab binding (Figures S1C and S1F), suggesting that the bivalent recognition of Env by CoRBS Abs is required to facilitate access to anti-cluster A Abs.

To determine the conformation recognized by anti-cluster A Abs, we performed smFRET imaging on HIV-1_{JR-FL} Env and Env ΔCT with donor and acceptor fluorophores attached to the V1 and V4 loops of gp120 (Munro et al., 2014). Introduction of the Q3 and A1 peptides into the V1 and V4 loops, respectively, minimally affected Env processing or stability (data not shown). Labeled virions were immobilized on quartz microscope slides and imaged using total internal reflection fluorescence (TIRF) microscopy. smFRET trajectories acquired from individual Env molecules indicated the same three FRET states previously reported: State 1 (0.18 ± 0.09), State 2 (0.65 ± 0.09), and State 3 (0.38 ± 0.09; Figures 1A and S2A). Incubation with a CD4mc led to a slight stabilization of State 3 in Env (Figures 1 and S2B) and to the emergence of a low but detectable occupancy in a fourth FRET state (0.84 ± 0.06). This state was detectable, although at very low levels, in unbound Env. Hidden Markov modeling (HMM) of the smFRET trajectories confirmed the existence of four distinct FRET states, as was also seen during visual inspection of the traces (Figure S3). The additional presence of the 17b Ab further stabilized State 3 and the fourth FRET state. The FRET value of the fourth state shifted subtly higher in the presence of 17b (0.90 ± 0.08; Figures 1C and S2C). This increase in the FRET value of the fourth state may indicate a further shift in Env conformation, which is not promoted by the small-molecule CD4mc alone and requires interaction with an Ab. Introduction of the A32 Ab in addition to the CD4mc and 17b dramatically stabilized the 0.9-FRET state (Figures 1 and S2). Similar results were obtained when the CD4mc was replaced by sCD4 (Figure S2E). The 17b Fab fragment was less effective than the complete 17b Ab in increasing the stability of the 0.9-FRET state (Figure 1D). Incubation of the labeled virus with C11 Ab, in the presence of CD4mc and 17b, showed a similar, although less dramatic, stabilization of 0.9 FRET and greater occupancy of State 3. In all cases, the effect of the anti-cluster A Abs was consistent regardless of the presence of the cytoplasmic tail of Env (Figure S2). Of note, HIV-1_{BG505} Env displayed similar stabilization of 0.9 FRET in the presence of CD4mc, 17b, and A32 (Figures S2G–S2J), indicating that our results are not limited to HIV-1_{JR-FL}.

HMM analysis indicated that transitions of unbound Env primarily occurred between States 2 and 3 as shown in a transition density plot (TDP), as previously reported (Ma et al., 2018; Munro et al., 2014). Transitions to the 0.9-FRET state increased upon the addition of 17b and further increased in the presence of the anti-cluster A Abs. Since most transitions to 0.9 FRET occurred from State 2 (Figure 1), we designate this conformation as State 2A. However, we cannot exclude the possibility that transient dwells in State 3 occurred that were not detectable at our current time resolution. Overall, these data support the presence of an additional conformational state of HIV-1 Env that is associated with anti-cluster A Ab binding in the presence of CD4mc and 17b.

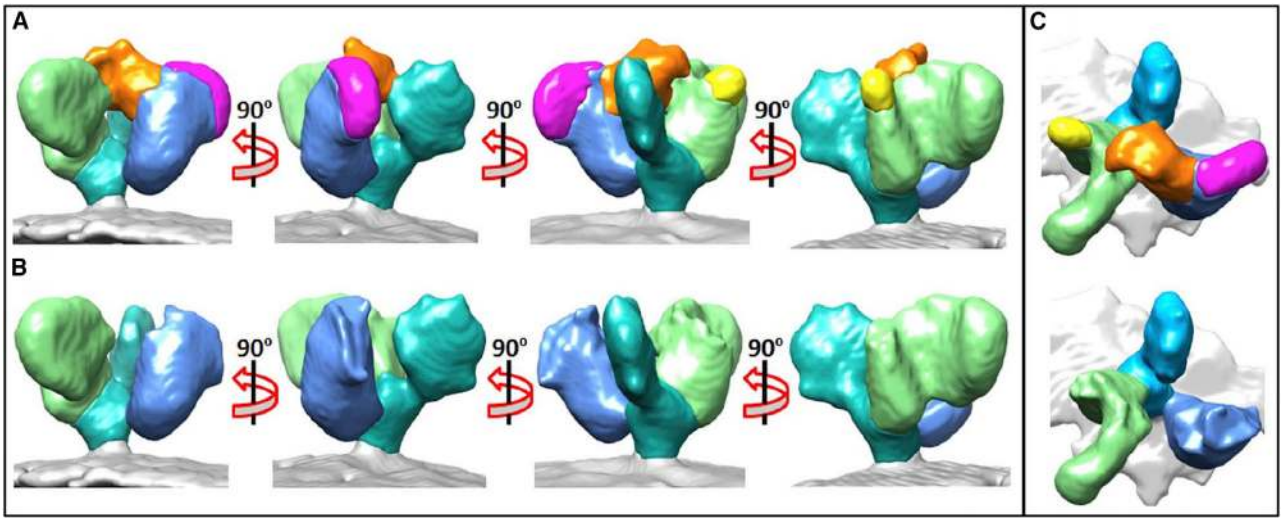

Figure 3. Modeling the HIV-1 Env Spike in State 2A

The left column shows the side views of segmented masked cryo-EM density (at ~13 Å resolution) of Env in complex with BNM-III-170 and the 17b and A32 antibodies. The Env-associated density is colored cyan, blue, and green, with the membrane colored gray.

(A) The upper panel represents the different side views of the complex projected at right angles. Orange, purple, and yellow colored regions exhibit the additional densities corresponding to parts of the bound-antibody Fab chains.

(B) Side views of the membrane-bound asymmetric HIV-1 spike projected at right angles, same as displayed in (A).

(C) Top views of the densities corresponding to (A) and (B).

Structural Characterization of Env State 2A by Cryo-EM

To gain a structural understanding of the conformation adopted by Env in the presence of CD4mc, anti-CoRBS, and cluster A Abs, we solved a ~13 Å resolution structure of Env present on the surface of Aldrithiol-2 (AT-2)-inactivated HIV-1 particles (Liu et al., 2008; Rossio et al., 1998) incubated with BNM-III-170, A32, and 17b Abs. Cryo-EM images show Env/BNM-III-170/17b/A32 on the surface of the viral particles (Figure 2). Two-dimensional alignment and classification showed class averages consistent with an asymmetric organization of the gp41-gp120 hetero-trimer (Figure S4). The three-dimensional structure of these complexes was determined using *in situ* single-particle image analysis (Figures 3A and S4). The asymmetric organization of gp120 was clearly visualized in the ~13 Å-resolution map (Figures 2 and 3). In addition to densities assigned to gp120 and gp41, additional densities were present in the final map (Figure 3). These densities could be assigned to three Fab chains in the model.

CD4 Downregulation Prevents the Spontaneous Sampling of State 2A

Both sCD4 and CD4mc fail to expose cluster A epitopes on their own (Figure S1). In contrast, membrane-bound CD4 exposes these epitopes without the cooperation of CoRBS Abs (Acharya et al., 2014; Veillette et al., 2014b). This unique ability of membrane-bound CD4 to expose cluster A epitopes explains why cells infected with nef-defective HIV-1 are readily recognized by anti-cluster A Abs. Indeed, in cells infected with nef-deleted viruses, CD4 accumulates at the cell surface and engages Env, readily exposing cluster A epitopes (Alsahafi et al., 2016; Prevost et al., 2018b; Veillette et al., 2014b, 2015). However, cells infected with a wild-type virus fail to expose cluster A epitopes, even in the presence of CD4mc (Richard et al., 2016). To achieve a better understanding of the conformation induced by the interaction with membrane-bound CD4, we produced HIV-1 particles using a nef-deleted virus in the absence or presence of membrane-bound CD4 and evaluated Env conformational dynamics by smFRET. We observed no effect of *nef* deletion on the conformational equilibrium of unliganded Env (compare Figures 4A, 1A, and S2A). In agreement with the ability of membrane-bound CD4 to directly expose cluster A epitopes, incorporation of CD4 into viral particles readily promoted transitions to open Env conformations. In particular, the stabilization of State 2A is consistent with the enhanced exposure of the cluster A epitopes. Altogether, these data suggest that Nef-mediated CD4 downregulation might be a mechanism to avoid exposure of the Ab-vulnerable State 2A conformation.

Impact of Proteolytic Processing on Env Conformational Dynamics

Previous reports have suggested that proteolytic processing decreases the conformational flexibility of Env, resulting in reduced exposure of certain CD4i epitopes (Chakrabarti et al., 2011; Haim et al., 2013). We therefore evaluated the impact of Env cleavage on A32 and C11 recognition. As shown in Figures 5A and 5B, preventing proteolytic processing of Env through mutation of the cleavage site (Env CL–) significantly enhanced recognition by anti-cluster A Abs, A32 and C11. A recent report suggested that the C11 epitope is buried deeper than A32 within the trimer (Tolbert et al., 2017). Accordingly, while 17b Ab and Fab′2 fragment were still required to expose the epitope recognized by C11, a single 17b-Fab fragment was sufficient to expose the epitope bound by A32 in Env CL- (Figures 5A and 5B). Apparently, the epitope recognized by A32 is exposed before the one

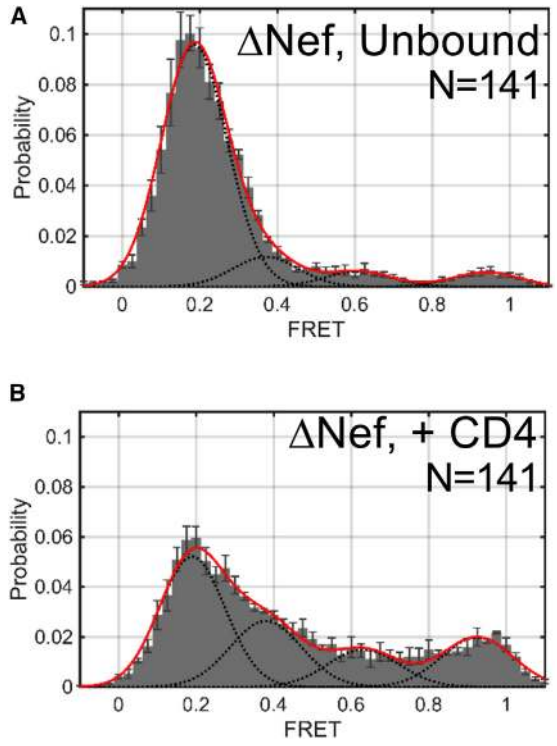

Figure 4. Membrane-Bound CD4 Exposes Cluster A Epitopes and Stabilizes Env State 2A

FRET histograms observed for HIV-1_{JR-FL} Env (A) in the absence of Nef and any bound ligand and (B) in the presence of membrane-bound CD4. Histograms are displayed as in Figure 1.

seen by C11, in agreement with previous observations (Tolbert et al., 2017). To confirm the impact that Env processing has on Env conformational dynamics, we performed smFRET analysis. As shown in Figure 5C, the unliganded Env CL- displayed greater intrinsic sampling of States 2 and 3 (41% combined occupancy) as compared to its cleaved counterpart (13% for Env and 18% for Env ΔCT; Figures 5C, 1A, and S2A), confirming greater conformational flexibility prior to cleavage. Addition of BNM-III-170 in combination with 17b, and either A32 or C11, resulted in a significant stabilization of State 2A (Figures 5D and 5E).

Antibodies Present in HIV+ Sera Can Stabilize State 2A in the Presence of CD4mc

It was previously shown that the small-molecule CD4mc BNM-III-170 enhances the susceptibility of HIV-1-infected cells to ADCC mediated by HIV+ sera (Richard et al., 2015, 2017). Importantly, this activity depends on the presence of anti-cluster A Abs (Ding et al., 2016; Tolbert et al., 2016), which we now know stabilize State 2A (Figures 1, 5, and S2). Therefore, to investigate whether HIV+ sera are able to stabilize State 2A, we first evaluated the ability of HIV+ sera from 9 chronically infected individuals, and 3 HIV− sera, for their ability to allow A32 recognition of HIV-1_{JR-FL} Env. As shown in Figure S5A, in the absence of the CD4mc BNM-III-170, A32 binding to HIV-1 Env-expressing cells was minimal, even in the presence of HIV+ sera. However, upon the addition of BNM-III-170, all HIV+ sera increased A32 recognition (Figure S5A). This suggests that HIV+ sera can stabilize State 2A in the presence of a CD4mc. Accordingly, smFRET analysis of HIV-1_{JRFL} Env in the presence of the same 9 HIV+ sera showed that while low levels of State-2A Envs were observed in the absence of CD4mc, the addition of the CD4mc increased the occupancy of State 2A by as much as nearly 8-fold (Figures 6A and 6C). In contrast, HIV− sera in the presence CD4mc did not promote State 2A beyond what was seen in the presence of CD4mc alone (compare Figure 6B with Figure 1B).

State 2A Is Susceptible to ADCC Responses

Previous reports indicated that anti-cluster A Abs mediate potent ADCC against cells expressing Env in the CD4-bound conformation (Alsahafi et al., 2016; Ding et al., 2016; Prevost et al., 2017; Prevost et al., 2018b; Richard et al., 2016; Veillette et al., 2014b, 2015). To evaluate whether the different conditions found here to stabilize State 2A resulted in enhanced susceptibility to ADCC, we incubated primary $CD4^+$ T cells infected with HIV-1_{JR-FL} together with the HIV+ sera exhibiting different degrees of State 2A stabilization activity (Figure 6A). We then evaluated their ability to mediate ADCC in the absence or presence of the CD4mc. All HIV+ sera mediated ADCC more efficiently upon CD4mc BNM-III-170 addition (Figure 7A) and to an extent that correlated with their ability to increase A32 recognition (Spearman's rank correlation r = 0.74; Figure S5B). Interestingly, the extent of serum-mediated ADCC was significantly decreased upon 17b or A32 Fab fragment addition (alone or in combination) (Figure 7A), in agreement with the requirement of the Fc-portion of both Abs to engage FcγRIIIa and mediate robust ADCC (Anand et al., 2018). These results agree with a model in which sequential opening of the trimer requires CoRBS Abs to expose cluster A epitopes (Richard et al., 2016). Of note, State 2A occupancy strongly correlated with the ability of HIV+ sera to recognize HIV-1-infected cells (Figure 7B) and with their capacity to interact with a recombinant stabilized gp120 inner domain that only exposes cluster A epitopes (Tolbert et al., 2016) (Figure 7C). These observations suggest that anti-cluster A Abs present in HIV+ sera help stabilize State 2A. Of note, we also observed that in the presence of the CD4mc BNM-III-170, 17b enabled the exposure of the A32 epitope at the surface of primary $CD4^+$ T cells isolated from viremic, untreated HIV-1-infected individuals (Figures S6A and S6B); thus, this Env conformation can be induced in biologically relevant samples. Finally, further supporting the susceptibility of State 2A to ADCC, we observed that Nef deletion, which results in the stabilization of State 2A in the presence of membrane-bound CD4 (Figure 4), significantly enhanced the susceptibility of infected cells to ADCC responses mediated by HIV+ sera (Figures S6C and S6D).

DISCUSSION

HIV-1 infection elicits a robust humoral immune response against the viral envelope glycoprotein. But the vast majority of the elicited Abs are non-neutralizing (nnAbs). These Abs target variable regions or conserved epitopes that are not exposed in the "closed" untriggered trimer (State 1). However, Env has intrinsic access to the "open" CD4-bound conformation (State 3) through one necessary conformational intermediate (State 2), in which only one protomer has bound CD4 (Ma et al., 2018; Munro

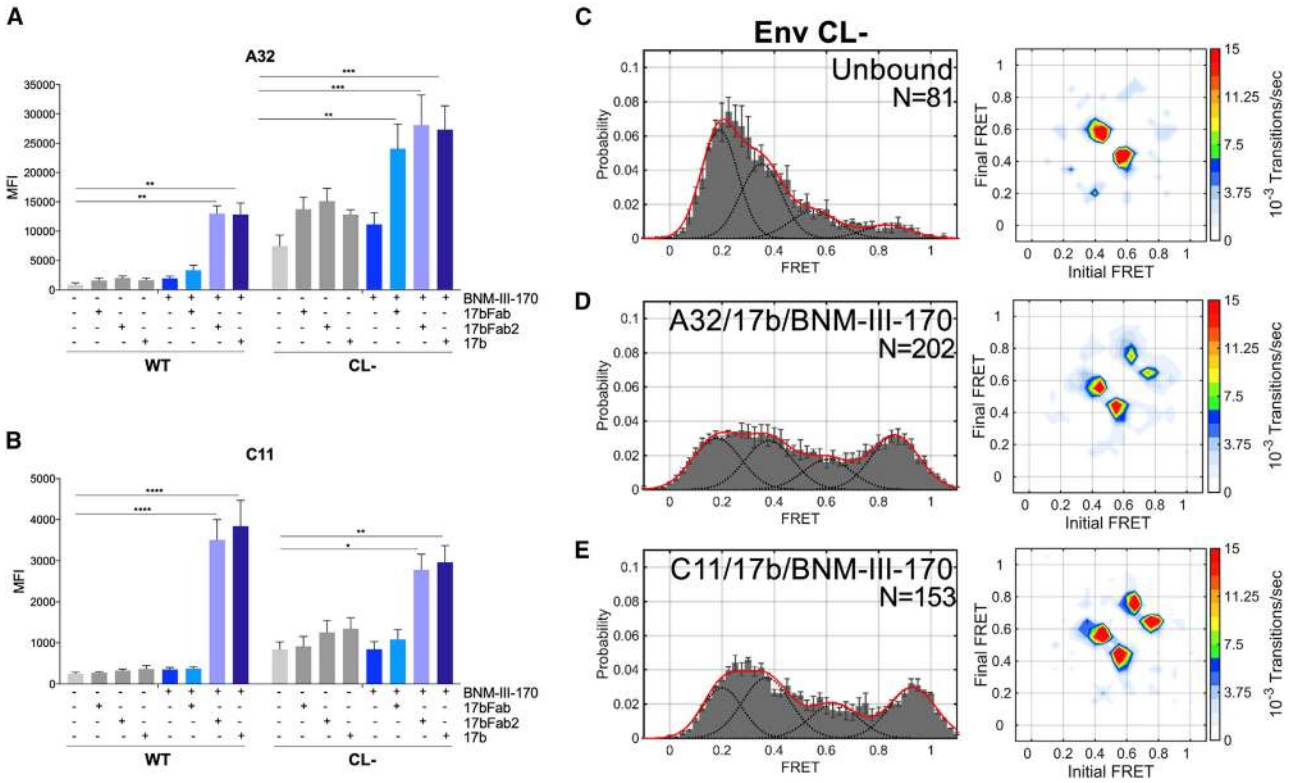

Figure 5. Env Cleavage Decreases the Spontaneous Sampling of State 2A

(A and B) The impact of Env cleavage on cluster A epitope exposure was evaluated in the presence or absence of the CD4mc BNM-III-170 and CoRBS 17b (full antibody or Fab or Fab′2 fragments) by cell-surface staining of 293 T cells transfected with HIV-1_{JRFL} ΔCT Env (CI+) or its cleavage defective (CI−) counterpart, using the A32 (A) or C11 (B) anti-cluster A Abs. Data are presented as means and SEM of the mean fluorescence intensity (MFI) from at least three independent experiments. Statistical significance was evaluated using multiple-comparison one-way ANOVAs or Kruskal-Wallis test, *$p < 0.05$, **$p < 0.01$, ***$p < 0.001$, ****$p < 0.0001$; ns, not significant.

(C–E) FRET histograms and TDPs for (C) unbound HIV-1_{JR-FL} CL− Env, and in the presence of (D) BNM-III-170, 17b Ab, and A32 Ab, or (E) BNM-III-170, 17b Ab, and C11 Ab. All ligands were used at the same concentrations as in Figure 1. FRET data are displayed as in Figure 1.

et al., 2014). Primary tier-2 viruses have Envs that are more "closed," with elevated State 1 occupancy, explaining why they are resistant to recognition by Abs (Ma et al., 2018; Munro et al., 2014). CD4 interaction modifies the conformational landscape, facilitating transitions to State 3 by lowering the energy barrier to the "open" states (Herschhorn et al., 2016; Ma et al., 2018; Munro et al., 2014). By exploring the Env conformational landscape in association with the epitopes recognized by different classes of CD4i Abs, we found that Env is able to sample a fourth conformation (State 2A; Figure S7). Env occupancy of States 2 and 3 can be enhanced with saturating concentrations of CD4mcs (Herschhorn et al., 2016). When Env samples these states, it can be recognized by CD4i Abs targeting the CoRBS and the V3 loop, but the cluster A epitopes remain obscured. Binding of CoRBS Abs, but not their Fab fragments, facilitates anti-cluster A Ab binding to Env (Figures 1 and S1). Thus, optimal stabilization of this asymmetric Env state apparently requires bivalent engagement of the CoRBS Abs. Accordingly, a ~13 Å resolution cryo-EM structure of Env in complex with the CD4mc BNM-III-170 and complete 17b and A32 Abs revealed an asymmetric Env conformation. This structure is consistent with a model where two gp120 subunits are bound by 17b Fab fragments potentially coming from the same Ab. This interaction liberates the third subunit, resulting in the exposure of the otherwise-buried A32 epitope. Higher resolution maps are required in order to unequivocally establish the identity of the Fab-binding fragments.

The difficulty of exposing the cluster A epitopes might explain why the unbound Env has low State 2A occupancy. Interestingly, anti-cluster A Abs are those that present the most potent ADCC activity among easily elicited CD4i Abs (Ding et al., 2016; Richard et al., 2016). It is therefore tempting to speculate that barriers limiting transitions to State 2A represent a viral mechanism to avoid exposure of vulnerable cluster A epitopes. Interestingly, while CD4mcs require the addition of CoRBS Abs to expose cluster A epitopes, we found that binding to membrane-bound CD4 is sufficient to trigger this conformation. These data are in agreement with previous reports that showed the critical role played by Nef-mediated CD4 downregulation in avoiding ADCC responses mediated by HIV+ sera and anti-cluster A Abs (Alsahafi et al., 2016; Prevost et al., 2018b; Veillette et al., 2014b, 2015). Our data also confirm the significant flexibility of the uncleaved HIV-1 Env, which is able to spontaneously sample all four states. Env cleavage shifts this conformational landscape,

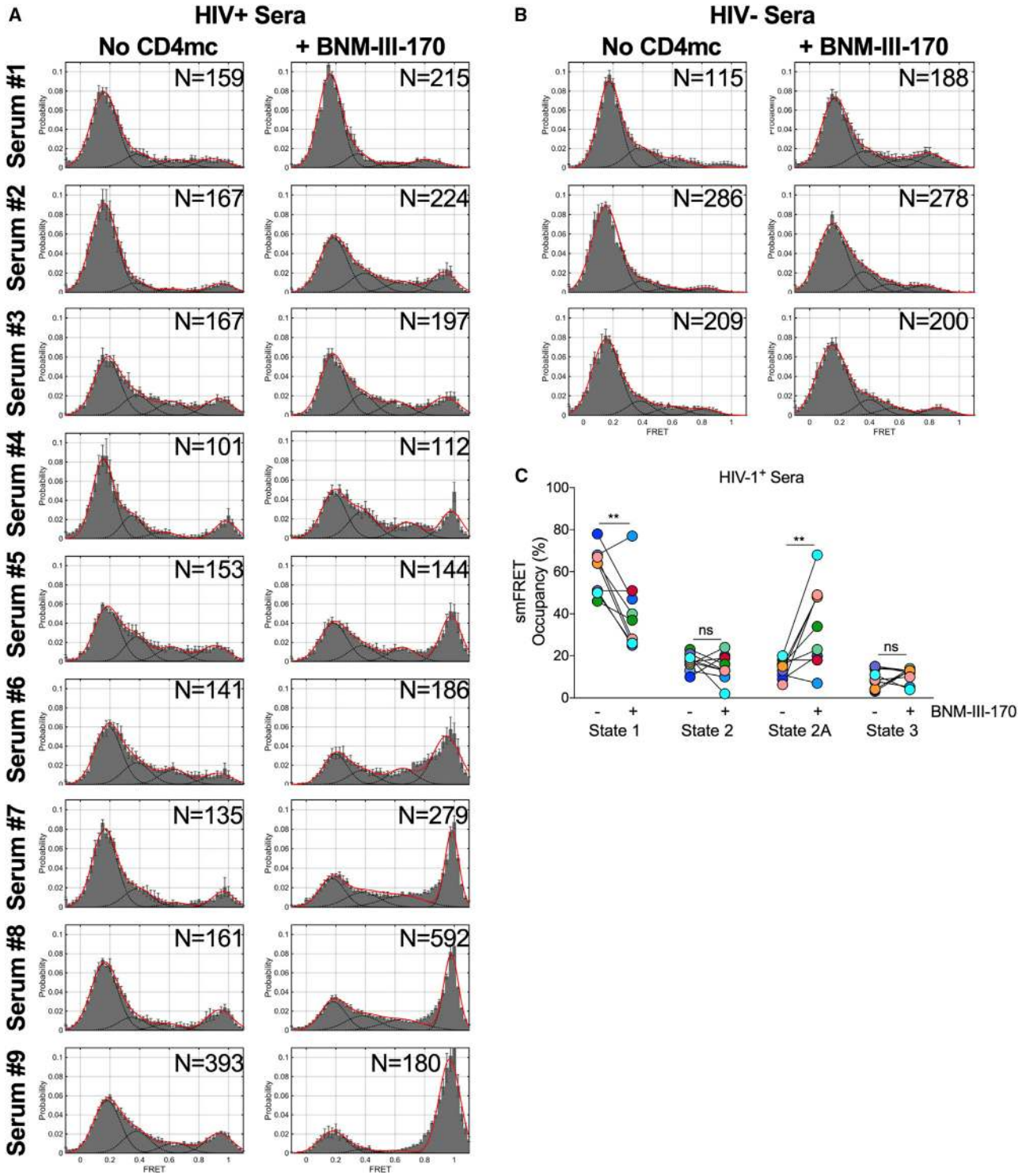

Figure 6. HIV+ Sera Stabilize State 2A in the Presence of CD4mc

(A and B) FRET histograms obtained for HIV-1_{JR-FL} Env ΔCT in the absence or presence of CD4mc BNM-III-170 (100 μM), as indicated, and in the presence of (A) sera from 9 chronically HIV-1-infected individuals or (B) 3 healthy uninfected individuals. FRET histograms are displayed as in Figure 1.

(C) The impact of CD4mc BNM-III-170 addition on FRET state occupancy for each of the 9 HIV+ sera. Statistical significance was evaluated using an unpaired t test or Mann-Whitney test, **$p < 0.01$; ns, not significant.

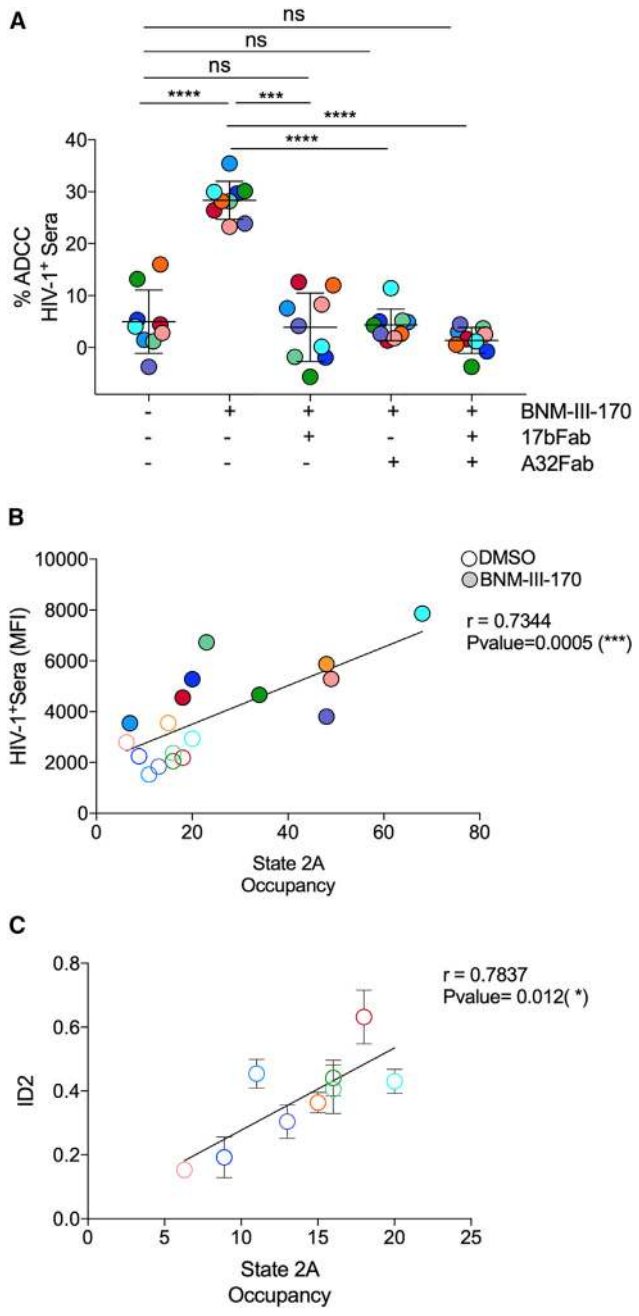

Figure 7. CD4mc-Mediated Exposure of Cluster A Epitopes Sensitizes HIV-1-Infected Primary CD4⁺ T Cells to ADCC and Correlates with State 2A Stabilization

(A) Primary CD4⁺ T cells infected with the HIV-1_{JRFL} infectious molecular clone were used to evaluate the susceptibility of infected cells to ADCC mediated by sera from nine chronically HIV-1-infected individuals in the presence of CD4mc BNM-III-170, alone or in combination with Fab fragments of 17b, A32, or both. (B and C) (B) State 2A occupancy (Figure 6) exhibited a positive correlation with the binding of sera from nine chronically HIV-1-infected individuals ± CD4mc BNM-III-170 to primary CD4 T cells infected with the HIV-1_{JRFL} infectious molecular clone and (C) to the stabilized gp120 inner domain (ID2) (Tolbert et al., 2016) by ELISA. Data are presented as means and SEM from at least three independent experiments. Statistical significance was evaluated utilizing a multiple-comparison one-way ANOVAs or a Pearson rank correlation, *p < 0.05, ***p < 0.001, ****p < 0.0001; ns, not significant.

favoring the untriggered, most neutralization-resistant State 1 conformation. It has been previously suggested that incorporation of uncleaved Env on the surface of viral particles could serve as a viral defense mechanism by exposing epitopes that do not induce neutralizing Abs. However, here we show that this could result in recognition by anti-cluster A Abs that are capable of mediating ADCC. Increasing the ratio of cleaved to uncleaved Env on the infected cell surface would thus facilitate HIV-1 escape from ADCC. Our results suggest that HIV-1 must achieve a fine balance between exposing non-neutralizing epitopes and eliciting ADCC responses. Altogether, our data identify a conformational state of HIV-1 Env that is vulnerable to attack by easy-to-elicit CD4i Abs. Strategies aimed at inducing or stabilizing this conformation represent interventional approaches to fight HIV-1 infection.

STAR★METHODS

Detailed methods are provided in the online version of this paper and include the following:

- KEY RESOURCES TABLE
- CONTACT FOR REAGENT AND RESOURCE SHARING
- EXPERIMENTAL MODEL AND SUBJECT DETAILS
  - Ethics Statement
  - Cell Lines and Isolation of Primary Cells
  - Sera
- METHOD DETAILS
  - Plasmids and Site-Directed Mutagenesis
  - Viral Production, Infections, *Ex Vivo* Amplification and Detection of Infected Cells
  - Antibodies
  - smFRET Imaging
  - Flow Cytometry Analysis of Cell-Surface Staining
  - ADCC FACS-Based Assay
  - ELISA
  - Cryo-EM Grid Preparation
  - Structural Model Building
- QUANTIFICATION AND STATISTICAL ANALYSIS
  - Analysis of Flow Cytometry Data
  - Analysis of smFRET Data
- DATA AND SOFTWARE AVAILABILITY

SUPPLEMENTAL INFORMATION

Supplemental Information can be found online at https://doi.org/10.1016/j.chom.2019.03.002.

ACKNOWLEDGMENTS

The authors thank Maolin Lu and Xiaochu Ma for helpful discussions and critical reading of the manuscript, the CRCHUM Flow Cytometry Platform, the FRQS AIDS and Infectious Diseases network, Mario Legault for cohort coordination and clinical samples, and Dennis Burton for the infectious molecular clone JRFL. We would like to thank Andrew Leis from the Bio21 Advanced Microscopy Facility (University of Melbourne). This work was supported by a CIHR foundation grant #352417 to A.F. Support for this work was also provided by NIH R01 to A.F. and M.P. (AI129769), A.F. and X.W. (AI122953), J.S. (AI124982), and NIAID R01 to M.P. (AI116274). This study was also supported by NIH AI100663 Center for HIV/AIDS Vaccine Immunology and Immunogen Design (CHAVI-ID) (D.E.K.; PI: Dennis Burton) and by R01-GM56550 to

A.B.S. Work by J.B.M. was supported by the NIH (1K22AI116262), the Gilead Sciences Research Scholars Program in HIV, and the Campbell Foundation for AIDS Research. A.F. is the recipient of a Canada Research Chair on Retroviral Entry #RCHS0235. N.A. is the recipient of a King Abdullah scholarship for higher education from the Saudi Government. J.R. is the recipient of a Mathilde Krim Fellowships in Basic Biomedical Research from AmfAR. S.D. is the recipient of an FRSQ postdoctoral fellowship award. D.E.K. is supported by an FRQS Senior Research Scholar Award. I.R. is supported by the STEM-M Stimulus Fund (University of Melbourne). We thank Jeffrey Lifson and Julian Bess for providing the AT-2 inactivated viral particles from the AIDS and Cancer Virus Program, and Leidos Biomedical Research, Inc./Frederick National Laboratory for Cancer Research supported with federal funds from the National Cancer Institute, NIH, under contract HHSN261200800001E. The funders had no role in study design, data collection and analysis, decision to publish, or preparation of the manuscript. The views expressed in this presentation are those of the authors and do not reflect the official policy or position of the Uniformed Services University, US Army, the Department of Defense, or the US Government.

AUTHOR CONTRIBUTIONS

A.F. and J.B.M. conceived the study. A.F., I.R., N.A., N.B., and J.B.M. designed experimental approaches. A.F. and J.B.M. wrote the paper. A.F., I.R., N.A., N.B., M.K., S.B., D.D., J.R., S.D., S.P.A., H.L., H.M., S.K., X.W., W.M., and J.B.M. performed, analyzed, and interpreted the experiments. W.D.T., A.B.S., M.P., and D.E.K. supplied novel reagents. All authors have read, edited, and approved the final manuscript.

DECLARATION OF INTERESTS

The authors declare no competing interests. J.B.M. and W.M. are inventors on a patent related to the application of smFRET imaging to HIV-1 Env (US patent number US9938324B2).

Received: August 23, 2018
Revised: December 3, 2018
Accepted: February 28, 2019
Published: April 10, 2019

SUPPORTING CITATIONS

The following references appear in the Supplemental Information: Sorzano et al. (2018); Kimanius et al. (2016).

REFERENCES

Acharya, P., Tolbert, W.D., Gohain, N., Wu, X., Yu, L., Liu, T., Huang, W., Huang, C.C., Kwon, Y.D., Louder, R.K., et al. (2014). Structural definition of an antibody-dependent cellular cytotoxicity response implicated in reduced risk for HIV-1 infection. J. Virol. *88*, 12895–12906.

Alsahafi, N., Ding, S., Richard, J., Markle, T., Brassard, N., Walker, B., Lewis, G.K., Kaufmann, D.E., Brockman, M.A., and Finzi, A. (2016). Nef proteins from HIV-1 elite controllers are inefficient at preventing antibody-dependent cellular cytotoxicity. J. Virol. *90*, 2993–3002.

Anand, S.P., Prevost, J., Baril, S., Richard, J., Medjahed, H., Chapleau, J.P., Tolbert, W.D., Kirk, S., Smith, A.B., III, Wines, B., et al. (2018). Two families of Env antibodies efficiently engage Fc-gamma receptors and eliminate HIV-1 infected cells. J. Virol. https://doi.org/10.1128/JVI.01823-18.

Bar, K.J., Tsao, C.Y., Iyer, S.S., Decker, J.M., Yang, Y., Bonsignori, M., Chen, X., Hwang, K.K., Montefiori, D.C., Liao, H.X., et al. (2012). Early low-titer neutralizing antibodies impede HIV-1 replication and select for virus escape. PLoS Pathog. *8*, e1002721.

Bosch, V., and Pawlita, M. (1990). Mutational analysis of the human immunodeficiency virus type 1 env gene product proteolytic cleavage site. J. Virol. *64*, 2337–2344.

Chakrabarti, B.K., Pancera, M., Phogat, S., O'Dell, S., McKee, K., Guenaga, J., Robinson, J., Mascola, J., and Wyatt, R.T. (2011). HIV type 1 Env precursor cleavage state affects recognition by both neutralizing and nonneutralizing gp41 antibodies. AIDS Res. Hum. Retroviruses *27*, 877–887.

Das, D.K., Govindan, R., Nikic-Spiegel, I., Krammer, F., Lemke, E.A., and Munro, J.B. (2018). Direct visualization of the conformational dynamics of single influenza hemagglutinin trimers. Cell *174*, 926–937.

de la Rosa-Trevín, J.M., Quintana, A., Del Cano, L., Zaldívar, A., Foche, I., Gutiérrez, J., Gómez-Blanco, J., Burguet-Castell, J., Cuenca-Alba, J., Abrishami, V., et al. (2016). Scipion: a software framework toward integration, reproducibility and validation in 3D electron microscopy. J. Struct. Biol. *195*, 93–99.

Decker, J.M., Bibollet-Ruche, F., Wei, X., Wang, S., Levy, D.N., Wang, W., Delaporte, E., Peeters, M., Derdeyn, C.A., Allen, S., et al. (2005). Antigenic conservation and immunogenicity of the HIV coreceptor binding site. J. Exp. Med. *201*, 1407–1419.

Ding, S., Veillette, M., Coutu, M., Prevost, J., Scharf, L., Bjorkman, P.J., Ferrari, G., Robinson, J.E., Sturzel, C., Hahn, B.H., et al. (2016). A highly conserved residue of the HIV-1 gp120 inner domain is important for antibody-dependent cellular cytotoxicity responses mediated by anti-cluster A antibodies. J. Virol. *90*, 2127–2134.

Fenton-May, A.E., Dibben, O., Emmerich, T., Ding, H., Pfafferott, K., Aasa-Chapman, M.M., Pellegrino, P., Williams, I., Cohen, M.S., Gao, F., et al. (2013). Relative resistance of HIV-1 founder viruses to control by interferon-alpha. Retrovirology *10*, 146.

Finzi, A., Xiang, S.H., Pacheco, B., Wang, L., Haight, J., Kassa, A., Danek, B., Pancera, M., Kwong, P.D., and Sodroski, J. (2010). Topological layers in the HIV-1 gp120 inner domain regulate gp41 interaction and CD4-triggered conformational transitions. Mol. Cell *37*, 656–667.

Fontaine, J., Chagnon-Choquet, J., Valcke, H.S., Poudrier, J., and Roger, M. (2011). High expression levels of B lymphocyte stimulator (BLyS) by dendritic cells correlate with HIV-related B-cell disease progression in humans. Blood *117*, 145–155.

Fontaine, J., Coutlee, F., Tremblay, C., Routy, J.P., Poudrier, J., and Roger, M. (2009). HIV infection affects blood myeloid dendritic cells after successful therapy and despite nonprogressing clinical disease. J. Infect. Dis. *199*, 1007–1018.

Gohain, N., Tolbert, W.D., Orlandi, C., Richard, J., Ding, S., Chen, X., Bonsor, D.A., Sundberg, E.J., Lu, W., Ray, K., et al. (2016). Molecular basis for epitope recognition by non-neutralizing anti-gp41 antibody F240. Sci. Rep. *6*, 36685.

Guan, Y., Pazgier, M., Sajadi, M.M., Kamin-Lewis, R., Al-Darmarki, S., Flinko, R., Lovo, E., Wu, X., Robinson, J.E., Seaman, M.S., et al. (2013). Diverse specificity and effector function among human antibodies to HIV-1 envelope glycoprotein epitopes exposed by CD4 binding. Proc. Natl. Acad. Sci. USA *110*, E69–E78.

Haim, H., Salas, I., and Sodroski, J. (2013). Proteolytic processing of the human immunodeficiency virus envelope glycoprotein precursor decreases conformational flexibility. J. Virol. *87*, 1884–1889.

Herschhorn, A., Ma, X., Gu, C., Ventura, J.D., Castillo-Menendez, L., Melillo, B., Terry, D.S., Smith, A.B., III, Blanchard, S.C., Munro, J.B., et al. (2016). Release of gp120 restraints leads to an entry-competent intermediate state of the HIV-1 envelope glycoproteins. mBio *7*.

International HIV Controllers Study, Pereyra, F., Jia, X., McLaren, P.J., Telenti, A., de Bakker, P.I., Walker, B.D., Ripke, S., Brumme, C.J., Pulit, S.L., et al. (2010). The major genetic determinants of HIV-1 control affect HLA class I peptide presentation. Science *330*, 1551–1557.

Juette, M.F., Terry, D.S., Wasserman, M.R., Altman, R.B., Zhou, Z., Zhao, H., and Blanchard, S.C. (2016). Single-molecule imaging of non-equilibrium molecular ensembles on the millisecond timescale. Nat. Methods *13*, 341–344.

Kamya, P., Boulet, S., Tsoukas, C.M., Routy, J.P., Thomas, R., Cote, P., Boulassel, M.R., Baril, J.G., Kovacs, C., Migueles, S.A., et al. (2011). Receptor-ligand requirements for increased NK cell polyfunctional potential in slow progressors infected with HIV-1 coexpressing KIR3DL1*h/*y and HLA-B*57. J. Virol. *85*, 5949–5960.

Kimanius, D., Forsberg, B.O., Scheres, S.H., and Lindahl, E. (2016). Accelerated cryo-EM structure determination with parallelisation using GPUs in RELION-2. Elife *5*.

Korber, B., Foley, B.T., Kuiken, C., Pillai, S.K., and Sodroski, J.G. (1998). Numbering positions in HIV relative to HXB2CG. Hum. Retroviruses AIDS *3*, 102–111.

Lalonde, J.M., Kwon, Y.D., Jones, D.M., Sun, A.W., Courter, J.R., Soeta, T., Kobayashi, T., Princiotto, A.M., Wu, X., Schon, A., et al. (2012). structure-based design, synthesis, and characterization of dual hotspot small-molecule HIV-1 entry inhibitors. J. Med. Chem. *55*, 4382–4396.

Liu, J., Bartesaghi, A., Borgnia, M.J., Sapiro, G., and Subramaniam, S. (2008). Molecular architecture of native HIV-1 gp120 trimers. Nature *455*, 109–113.

Ma, X., Lu, M., Gorman, J., Terry, D.S., Hong, X., Zhou, Z., Zhao, H., Altman, R.B., Arthos, J., Blanchard, S.C., et al. (2018). HIV-1 Env trimer opens through an asymmetric intermediate in which individual protomers adopt distinct conformations. Elife *7*.

Madani, N., Princiotto, A.M., Zhao, C., Jahanbakhshsefidi, F., Mertens, M., Herschhorn, A., Melillo, B., Smith, A.B., III, and Sodroski, J. (2017). Activation and inactivation of primary human immunodeficiency virus envelope glycoprotein trimers by CD4-mimetic compounds. J. Virol. *91*.

Melillo, B., Liang, S., Park, J., Schon, A., Courter, J.R., LaLonde, J.M., Wendler, D.J., Princiotto, A.M., Seaman, M.S., Freire, E., et al. (2016). Small-molecule CD4-mimics: structure-based optimization of HIV-1 entry inhibition. ACS Med. Chem. Lett. *7*, 330–334.

Munro, J.B., Gorman, J., Ma, X., Zhou, Z., Arthos, J., Burton, D.R., Koff, W.C., Courter, J.R., Smith, A.B., III, Kwong, P.D., et al. (2014). Conformational dynamics of single HIV-1 envelope trimers on the surface of native virions. Science *346*, 759–763.

Ochsenbauer, C., Edmonds, T.G., Ding, H., Keele, B.F., Decker, J., Salazar, M.G., Salazar-Gonzalez, J.F., Shattock, R., Haynes, B.F., Shaw, G.M., et al. (2012). Generation of transmitted/founder HIV-1 infectious molecular clones and characterization of their replication capacity in CD4 T lymphocytes and monocyte-derived macrophages. J. Virol. *86*, 2715–2728.

Pacheco, B., Alsahafi, N., Debbeche, O., Prevost, J., Ding, S., Chapleau, J.P., Herschhorn, A., Madani, N., Princiotto, A., Melillo, B., et al. (2017). Residues in the gp41 ectodomain regulate HIV-1 envelope glycoprotein conformational transitions induced by gp120-directed inhibitors. J Virol. *91*.

Parrish, N.F., Gao, F., Li, H., Giorgi, E.E., Barbian, H.J., Parrish, E.H., Zajic, L., Iyer, S.S., Decker, J.M., Kumar, A., et al. (2013). Phenotypic properties of transmitted founder HIV-1. Proc. Natl. Acad. Sci. USA *110*, 6626–6633.

Peretz, Y., Ndongala, M.L., Boulet, S., Boulassel, M.R., Rouleau, D., Cote, P., Longpre, D., Routy, J.P., Falutz, J., Tremblay, C., et al. (2007). Functional T cell subsets contribute differentially to HIV peptide-specific responses within infected individuals: correlation of these functional T cell subsets with markers of disease progression. Clin. Immunol. *124*, 57–68.

Pettersen, E.F., Goddard, T.D., Huang, C.C., Couch, G.S., Greenblatt, D.M., Meng, E.C., and Ferrin, T.E. (2004). UCSF Chimera–a visualization system for exploratory research and analysis. J. Comp. Chem. *25*, 1605–1612.

Pintilie, G.D., Zhang, J., Goddard, T.D., Chiu, W., and Gossard, D.C. (2010). Quantitative analysis of cryo-EM density map segmentation by watershed and scale-space filtering, and fitting of structures by alignment to regions. J. Struct. Biol. *170*, 427–438.

Prevost, J., Zoubchenok, D., Richard, J., Veillette, M., Pacheco, B., Coutu, M., Brassard, N., Parsons, M.S., Ruxrungtham, K., Bunupuradah, T., et al. (2017). Influence of the envelope gp120 Phe 43 cavity on HIV-1 sensitivity to antibody-dependent cell-mediated cytotoxicity responses. J Virol. *91*.

Prevost, J., Richard, J., Ding, S., Pacheco, B., Charlebois, R., Hahn, B.H., Kaufmann, D.E., and Finzi, A. (2018a). Envelope glycoproteins sampling states 2/3 are susceptible to ADCC by sera from HIV-1-infected individuals. Virology *515*, 38–45.

Prevost, J., Richard, J., Medjahed, H., Alexander, A., Jones, J., Kappes, J.C., Ochsenbauer, C., and Finzi, A. (2018b). Incomplete downregulation of CD4 expression affects HIV-1 Env conformation and antibody-dependent cellular cytotoxicity responses. J Virol. *92*.

Richard, J., Veillette, M., Batraville, L.A., Coutu, M., Chapleau, J.P., Bonsignori, M., Bernard, N., Tremblay, C., Roger, M., Kaufmann, D.E., et al. (2014). Flow cytometry-based assay to study HIV-1 gp120 specific antibody-dependent cellular cytotoxicity responses. J. Virol. Methods *208*, 107–114.

Richard, J., Veillette, M., Brassard, N., Iyer, S.S., Roger, M., Martin, L., Pazgier, M., Schon, A., Freire, E., Routy, J.P., et al. (2015). CD4 mimetics sensitize HIV-1-infected cells to ADCC. Proc. Natl. Acad. Sci. USA *112*, E2687–E2694.

Richard, J., Pacheco, B., Gohain, N., Veillette, M., Ding, S., Alsahafi, N., Tolbert, W.D., Prevost, J., Chapleau, J.P., Coutu, M., et al. (2016). Co-receptor binding site antibodies enable CD4-mimetics to expose conserved anti-cluster A ADCC epitopes on HIV-1 envelope glycoproteins. EBioMedicine *12*, 208–218.

Richard, J., Prevost, J., von Bredow, B., Ding, S., Brassard, N., Medjahed, H., Coutu, M., Melillo, B., Bibollet-Ruche, F., Hahn, B.H., et al. (2017). BST-2 expression modulates small CD4-mimetic sensitization of HIV-1-infected cells to antibody-dependent cellular cytotoxicity. J. Virol. *91*.

Richard, J., Baxter, A.E., von Bredow, B., Ding, S., Medjahed, H., Delgado, G.G., Brassard, N., Stürzel, C.M., Kirchhoff, F., Hahn, B.H., et al. (2018). Uninfected bystander cells impact the measurement of HIV-specific ADCC responses. mBio *9*.

Rossio, J.L., Esser, M.T., Suryanarayana, K., Schneider, D.K., Bess, J.W., Jr., Vasquez, G.M., Wiltrout, T.A., Chertova, E., Grimes, M.K., Sattentau, Q., et al. (1998). Inactivation of human immunodeficiency virus type 1 infectivity with preservation of conformational and functional integrity of virion surface proteins. J. Virol. *72*, 7992–8001.

Schon, A., Madani, N., Klein, J.C., Hubicki, A., Ng, D., Yang, X., Smith, A.B., III, Sodroski, J., and Freire, E. (2006). Thermodynamics of binding of a low-molecular-weight CD4 mimetic to HIV-1 gp120. Biochemistry *45*, 10973–10980.

Si, Z., Madani, N., Cox, J.M., Chruma, J.J., Klein, J.C., Schon, A., Phan, N., Wang, L., Biorn, A.C., Cocklin, S., et al. (2004). Small-molecule inhibitors of HIV-1 entry block receptor-induced conformational changes in the viral envelope glycoproteins. Proc. Natl. Acad. Sci. USA *101*, 5036–5041.

Sorzano, C.O.S., Vargas, J., de la Rosa-Trevin, J.M., Jimenez, A., Maluenda, D., Melero, R., Martinez, M., Ramirez-Aportela, E., Conesa, P., Vilas, J.L., et al. (2018). A new algorithm for high-resolution reconstruction of single particles by electron microscopy. J. Struct. Biol. *204*, 329–337.

Tolbert, W.D., Gohain, N., Veillette, M., Chapleau, J.P., Orlandi, C., Visciano, M.L., Ebadi, M., DeVico, A.L., Fouts, T.R., Finzi, A., et al. (2016). Paring down HIV Env: design and crystal structure of a stabilized inner domain of HIV-1 gp120 displaying a major ADCC target of the A32 region. Structure *24*, 697–709.

Tolbert, W.D., Gohain, N., Alsahafi, N., Van, V., Orlandi, C., Ding, S., Martin, L., Finzi, A., Lewis, G.K., Ray, K., et al. (2017). Targeting the late stage of HIV-1 entry for antibody-dependent cellular cytotoxicity: structural basis for env epitopes in the C11 region. Structure *25*, 1719–1731.

Veillette, M., Coutu, M., Richard, J., Batraville, L.A., Desormeaux, A., Roger, M., and Finzi, A. (2014a). Conformational evaluation of HIV-1 trimeric envelope glycoproteins using a cell-based ELISA assay. J. Vis. Exp. *14*, 51995.

Veillette, M., Desormeaux, A., Medjahed, H., Gharsallah, N.E., Coutu, M., Baalwa, J., Guan, Y., Lewis, G., Ferrari, G., Hahn, B.H., et al. (2014b). Interaction with cellular CD4 exposes HIV-1 envelope epitopes targeted by antibody-dependent cell-mediated cytotoxicity. J. Virol. *88*, 2633–2644.

Veillette, M., Coutu, M., Richard, J., Batraville, L.A., Dagher, O., Bernard, N., Tremblay, C., Kaufmann, D.E., Roger, M., and Finzi, A. (2015). The HIV-1 gp120 CD4-bound conformation is preferentially targeted by antibody-dependent cellular cytotoxicity-mediating antibodies in Sera from HIV-1-infected individuals. J. Virol. *89*, 545–551.

von Bredow, B., Arias, J.F., Heyer, L.N., Moldt, B., Le, K., Robinson, J.E., Zolla-Pazner, S., Burton, D.R., and Evans, D.T. (2016). Comparison of antibody-dependent cell-mediated cytotoxicity and virus neutralization by HIV-1 Env-specific monoclonal antibodies. J. Virol. *90*, 6127–6139.

Wu, X., Parast, A.B., Richardson, B.A., Nduati, R., John-Stewart, G., Mbori-Ngacha, D., Rainwater, S.M., and Overbaugh, J. (2006). Neutralization escape variants of human immunodeficiency virus type 1 are transmitted from mother to infant. J. Virol. *80*, 835–844.

STAR★METHODS

KEY RESOURCES TABLE

REAGENT or RESOURCE	SOURCE	IDENTIFIER
Antibodies		
Anti-HIV-1 monoclonal A32, 17b, 19b	Dr. Andrés Finzi	N/A
Anti-HIV-1 monoclonal C11, N12-i2	Dr. Marzena Pazgier	N/A
Monoclonal anti-CD4 OKT4	eBiosciences	Cat# 14-0048-82
Anti-HIV-1 monoclonal GE2 JG8	Dr. Gunilla Karlsson Hedestam	N/A
Goat-anti-human Alexa -Flour 647	Invitrogen	Cat# A-21445
Goat-anti-mouse Alexa -Flour 647	Invitrogen	Cat# A32728
Anti-HIV-1 Fab fragments	Dr. Marzena Pazgier	N/A
Anti-HIV-1 Fab'2 fragments	Dr. Marzena Pazgier	N/A
Anti-HIV-1 monoclonal p24-KC57	Beckman Coulter /Immunotech	Cat# CO6604667
Horseradish peroxidase-conjugated (HRP)-human IgG	Thermo Fisher Scientific	Cat# P131413
Bacterial and Virus Strains		
Transmitted Founder (T/F) IMC CH58	Ochsenbauer et al., 2012; Bar et al., 2012; Parrish et al., 2013; Fenton-May et al., 2013; Richard et al., 2015	N/A
HIV-1 JRFL infectious molecular clone	Dr. Dennis Burton	N/A
Aldrithol-2 (AT-2) inactivated HIV-1_{Bal} viral particles	Dr Jeffrey Lifson	N/A
Biological Samples		
Sera from HIV-infected and uninfected donors	FRQS AIDS network	N/A
Primary human PBMCs, and primary CD4+ T cells	FRQS AIDS network	N/A
Chemicals, Peptides, and Recombinant Proteins		
phytohemagglutinin-L (PHA-L)	Sigma	Cat# L2769
rIL-2	NIH AIDS Reagent Program	Cat# 136
HIV-1gp120 inner domain (ID2)	Tolbert et al., 2016	N/A
CD4mimetic BNM-III-170	Melillo et al., 2016	N/A
sCD4	Dr. Andrés Finzi	N/A
Dimethyl sulfoxide (DMSO)	Thermo Fisher Scientific	Cat# BP2311
Phosphate buffered saline (PBS)	Wisent INC	Cat# 311-010
Bovine Serum Albumin (BSA)	BioShop	Cat# ALB001.100
Tris-buffered saline (TBS)	Thermo Fisher Scientific	Cat# BP24711
Western Lightning oxidizing and luminol reagents	Perkin Elmer Life Sciences	Cat# NEL105001EA
Tween-20	Thermo Fisher Scientific	Cat# BP337-500
DSPE-PEG^{2000}-biotin	Avanti Polar Lipids	Cat# 880129P
LD550-CoA	Lumidyne Technologies	N/A
LD650-CoA	Lumidyne Technologies	N/A
Streptavidin	Invitrogen	Cat# S888
Trypsin	Gibco	Cat# 253000-054
L-glutamine	Gibco	Cat# 25030-081
DMEM	Gibco	Cat# 11995065
OptiMEM	Gibco	Cat# 31985-070
RPMI 1640	Life Technology	Cat#11875093
Lipofectamine	Invitrogen	Cat# 100022052
Opti-prep	Sigma	Cat# D1556

(*Continued on next page*)

Continued

REAGENT or RESOURCE	SOURCE	IDENTIFIER
Fetal bovine serum	Gemini BioProducts	Cat# 100-106
Fetal bovine serum	VWR	NUL
Penicillin/streptomycin	Gibco	Cat# 15140-122
PEG-passivated, streptavidin-coated quartz slides	This paper	N/A
Trolox	Sigma	Cat# 238813
Cyclooctatetraene	Sigma	Cat# 138924
Nitrobenzyl alcohol	Sigma	Cat# N12821
Protocatechuic acid	Sigma	Cat# 37580
Protoatechuate 3,4-deoxygenase	Sigma	Cat# P8279
Formaldehyde-37%	Thermo Fisher Scientific	Cat# F79-500
Cell proliferation dye eFluor670	eBioscience	Cat# 65084085
Cell proliferation dye eFluor450	eBioscience	Cat# 65084285
AquaVivid	Thermo Fisher Scientific	Cat# L43957
Critical Commercial Assays		
EasySep Human $CD4^+$ T cell Enrichment Kit	StemCell Technologies	Cat# 19052
Alexa Fluor-647 Antibody Labeling Kit	Invitrogen	Cat# A20186
Cytofix/Cytoperm Fixation/ Permeabilization Kit	BD Biosciences	Cat# 554714
Deposited Data		
HIV-1_{BaL} Env bound to BNM-III-170, 17b, and A32	This study	EMDataBank: EMD-0466
Experimental Models: Cell Lines		
HEK293T human embryonic kidney cells	ATCC	Cat# CRL-3216
Recombinant DNA		
pcDNA3.1-clade B HIV-1_{JRFL}Env	Wu et al., 2006	N/A
pCAGGS -clade B HIV-1_{JRFL}Env	San Diego Biomedical Research Institute (Dr. James Binley)	N/A
pIRES-GFP vector	Simon Fraser University (Dr. Mark Brockman)	N/A
Plasmid encoding HIV-1_{BG505}	Fred Hutchinson Cancer Research Center (Dr. Julie Overbaugh)	N/A
Plasmid encoding HIV-$1_{JR\text{-}FL}$ Env with Q3 and A1 peptide inserts	Munro et al., 2014	N/A
Plasmid encoding HIV-1_{BG505} with Q3 and A1 peptide inserts in Env	Ma et al., 2018	N/A
pNL4-3 ΔEnv ΔRT	Munro et al., 2014	N/A
Software and Algorithms		
FlowJo vX.0.7	Tree Star	https://www.flowjo.com/solutions/flowjo/downloads
GraphPad Prism version 6.01	GraphPad	https://www.graphpad.com/scientific-software/prism/
Matlab	Mathworks	https://www.mathworks.com
Spartan	Weill Cornell Medical College (Dr. Scott Blanchard)	https://www.scottblanchardlab.com/software
Scipion	Spanish National Center for Biotechnology	http://scipion.i2pc.es; RRID: SCR_016738
Relion	MRC Laboratory of Molecular Biology	http://www2.mrc-lmb.cam.ac.uk/relion; RRID: SCR_016274
Chimera	University of California, San Francisco	http://plato.cgl.ucsf.edu/chimera; RRID: SCR_004097

(*Continued on next page*)

Continued

REAGENT or RESOURCE	SOURCE	IDENTIFIER
Other		
Thermo Fisher Scientific Talos Arctica equipped with a Gatan quantum 965 energy filter with a K2 direct detector	https://microscopy.unimelb.edu.au/	N/A
Quantifoil R2/2 grids	Quantifoil	N/A
LSRII cytometer	BD Biosciences	N/A
LB 941 TriStar luminometer	Berthold Technologies	N/A

CONTACT FOR REAGENT AND RESOURCE SHARING

Further information and requests for resources and reagents should be directed to and will be fulfilled by the Lead Contact, James B. Munro (james.munro@tufts.edu).

EXPERIMENTAL MODEL AND SUBJECT DETAILS

Ethics Statement

Written informed consent was obtained from all study participants [the Montreal Primary HIV Infection Cohort (Fontaine et al., 2009, 2011) and the Canadian Cohort of HIV Infected Slow Progressors (International HIV Controllers Study et al., 2010; Kamya et al., 2011; Peretz et al., 2007)], and research adhered to the ethical guidelines of CRCHUM and was reviewed and approved by the CRCHUM institutional review board (ethics committee, approval number CE 16.164 - CA). Research adhered to the standards indicated by the Declaration of Helsinki. All participants were adult and provided informed written consent prior to enrolment in accordance with Institutional Review Board approval.

Cell Lines and Isolation of Primary Cells

HEK293T human embryonic kidney cells (obtained from ATCC) were grown as previously described (Richard et al., 2015; Veillette et al., 2014b). HEK293T cells were derived from female human embryonic kidney cells, into which the simian virus 40 T-antigen was inserted. Primary human PBMCs, and CD4+ T cells were isolated, activated and cultured as previously described (Richard et al., 2015; Veillette et al., 2014b). Briefly, PBMCs were obtained by leukapheresis from 7 HIV-uninfected healthy adult (6 males, 1 female) donors. CD4+ T lymphocytes were purified from resting PBMCs by a negative selection using immunomagnetic beads per the manufacturer's instructions (StemCell Technologies, Vancouver, BC). CD4+ T lymphocytes were activated with phytohemagglutinin-L (10 μg/ mL) for 48 hours and then maintained in RPMI 1640 complete medium supplemented with rIL-2 (100 U/mL). Primary CD4 T cells were isolated from PBMCs obtained from 7 viremic untreated HIV-1-infected individuals (5 males, 2 females). Purified CD4+ T cells were activated with PHA-L at 10 μg /ml for 36 hours and then cultured for 6 days in RPMI-1640 complete medium supplemented with rIL-2 (100U/ml).

Sera

Sera from nine deidentified untreated HIV-infected (8 males, 1 female) and three HIV-uninfected healthy adult male donors were heat-inactivated and conserved as previously described (Richard et al., 2015; Veillette et al., 2014b).

METHOD DETAILS

Plasmids and Site-Directed Mutagenesis

The sequence of full-length clade B HIV-1_{JRFL} Env (Wu et al., 2006) was codon-optimized (GenScript) and cloned into the expression plasmid pcDNA3.1 or PCGGS. Site-directed mutagenesis was performed using the QuikChange II XL site-directed mutagenesis protocol (Stratagene), and a stop codon was introduced to replace the codon for Gly 711, truncating the cytoplasmic tail (ΔCT) and enhancing cell-surface expression of selected HIV-1_{JRFL} Env. Point mutations were introduced at positions R508S and R511S to allow changes on the gp120-gp41 cleavage site (Bosch and Pawlita, 1990). Mutations were either added individually or in combination into pcDNA3.1-JRFL Env or the PCGGS-JRFL Env. The presence of the desired mutations was determined by automated DNA sequencing. The numbering of the HIV-1 Env amino acid residues is based on that of the prototypic HXBc2 strain of HIV-1, where position 1 is the initial methionine (Korber et al., 1998).

Viral Production, Infections, *Ex Vivo* Amplification and Detection of Infected Cells

HIV-1 viruses were produced and titrated as previously described (Veillette et al., 2015). Viruses were then used to infect activated primary CD4 T cells by spin infection at 800 × *g* for 1 h in 96-well plates at 25 °C. In order to expand endogenously-infected CD4 T cells, primary CD4 T cells were isolated from PBMCs from HIV-1-infected individuals. Purified $CD4^+$ T cells were activated with

PHA-L at 10 μg/ml for 36 hours and then cultured for 6 to 8 days in RPMI-1640 complete medium supplemented with rIL-2 (100 U/ml) (Richard et al., 2015).

Antibodies

Anti-HIV-1 cluster A monoclonal antibodies A32, and C11 were either conjugated with Alexa-Flour 647 probe (Invitrogen) or not and used for cell-surface staining of HIV-1 Env expressing cells. The following Abs were used alone or in combination with anti-cluster A mAbs for cell-surface staining: A32, C11, 17b, 19b, GE2JG8, N12-i2, (1μg/ml) and the Fab fragments, Fab'2 fragments or full 17b (5μg/ml) mAb. The monoclonal anti-CD4 OKT4 (1μg/ml) (14-0048-82; eBiosciences) was used to measure cell surface levels of CD4, as previously shown (Richard et al., 2015). The secondary goat anti-mouse and anti-human antibodies coupled to Alexa Fluor 647 (Invitrogen) were used as secondary Abs.

smFRET Imaging

HIV-1_{JR-FL} virions with a single peptide-tagged gp120 domain were generated, purified, and fluorescently labeled as described (Munro et al., 2014). Briefly, HEK293T cells were transfected with pNL4-3 ΔEnv ΔRT plasmid, and a 20:1 ratio of wild-type HIV-1_{JR-FL} gp160 plasmid to gp160 with the V1-Q3 and V4-A1 peptide insertions. Virus was collected 24 hours post-transfection and pelleted in PBS over a 5% sucrose cushion at 20,000x g for 2 hours. The virus was resuspended in labeling buffer (50 mM HEPES pH7, 10 mM $CaCl_2$, 10 mM $MgCl_2$), and incubated overnight at room temperature with 0.5 μM each of LD550-cadaverine and LD650-coenzyme A (Lumidyne Technologies), 0.65 μM transglutaminase (Sigma), and 5 μM acyl carrier protein synthase (AcpS), which labels the Q3 and A1 peptides, respectively. The virus was then incubated with 0.02 mg/ml DSPE-PEG_{2000}-biotin (Avanti Polar Lipids) for 30 minutes at room temperature with gentle mixing. Virus was purified away from unbound fluorophore and lipid by ultracentrifugation over a 5%-20% Optiprep (Sigma) gradient in an SW41 rotor (Beckman Coulter) for 1 hour at 35,000 rpms. The gradients were fractionated and the fractions containing labeled HIV-1_{JR-FL} virions were identified by p24 Western blot, pooled, and stored at -80°C until use in imaging experiments. Virus preparations with HIV-1_{JR-FL} Env ΔCT or Env CL-, or with HIV-1_{BG505} Env were generated in exactly the same manner. The purified labeled virions were immobilized on passivated, streptavidin-coated quartz microscope slides. smFRET imaging was performed on a custom-built prism-based TIRF microscope controlled by Micro-Manager software (Open Imaging) as described (Das et al., 2018). All ligands were introduced to the labeled virus and incubated for 1 hour at room temperature prior to surface immobilization.

Flow Cytometry Analysis of Cell-Surface Staining

To assess the Env conformation of wild-type codon-optimized HIV-1_{JR-FL} Env by flow cytometry analysis, 3 X 10^5 293T cells were transfected by the calcium phosphate method with the Env-expressing plasmids along with a pIRES-GFP vector, at a ratio of 2 μg of pcDNA3.1 or JRFL ΔCT Env variants to 0.5 μg of green fluorescence protein (GFP). Sixteen hours post-transfection, cells were washed with fresh medium and epitope exposure was evaluated 24 h later. The recombinant Alexa-Fluor-conjugated C34-Ig protein (Si et al., 2004) was used to detect HR1 exposure in the presence or absence of sCD4 (10μg/ml), as previously shown (Pacheco et al., 2017).

Cell-surface staining was performed as previously described (Richard et al., 2015; Veillette et al., 2015). Binding of HIV-1-Env expressing cells by sera (1:1000 dilution), anti-Env mAbs or anti-CD4 mAbs was performed with or without BNM-III-170 (50μM) or its equivalent volume of vehicle (DMSO) at 48h post-infection/transfection. Cells infected with HIV-1 primary isolates were stained intracellularly for HIV-1 p24, using the Cytofix/Cytoperm Fixation/ Permeabilization Kit (BD Biosciences, Mississauga, ON, Canada) and the fluorescent anti-p24 mAb (PE-conjugated anti-p24, clone KC57; Beckman Coulter/Immunotech). The percentage of infected or transfected cells ($p24^+$ cells or GFP^+, respectively) was determined by gating the living cell population on the basis of the AquaVivid viability dye staining. Samples were analyzed on an LSRII cytometer (BD Biosciences), and data analysis was performed using FlowJo vX.0.7 (Tree Star, Ashland, OR, USA).

ADCC FACS-Based Assay

Measurement of ADCC using the FACS-based assay was performed at 48h post-infection as previously described (Richard et al., 2014, 2015, 2018; Veillette et al., 2014b). Briefly, infected primary $CD4^+$ T cells were stained with viability (AquaVivid; Thermo Fisher Scientific) and cellular (cell proliferation dye eFluor670; eBioscience) markers and used as target cells. Autologous PBMC effectors cells, stained with another cellular marker (cell proliferation dye eFluor450; eBioscience), were added at an effector: target ratio of 10:1 in 96-well V-bottom plates (Corning, Corning, NY). Briefly, infected primary $CD4^+$ T cells were incubated with autologous PBMC (Effector: Target ratio of 10:1) in presence of A32 (0.3125, 0,625, 1,25, 2,5 or 5 μg/ml,) and 17b (5 μg/ml) or17b Fab fragments alone or in combination, or with HIV+ sera (1:1000), in presence of 50 μM of BNM-III-170 or with equivalent volume of vehicle (DMSO). The plates were subsequently centrifuged for 1 min at 300 g, and incubated at 37°C, 5% CO_2 for 5 to 6 h before being fixed in a 2% PBS-formaldehyde solution. Samples were analyzed on an LSRII cytometer (BD Biosciences). Data analysis was performed using FlowJo vX.0.7 (Tree Star). The percentage of ADCC was calculated with the following formula: (% of p24+ cells in Targets plus Effectors) − (% of p24+ cells in Targets plus Effectors plus sera) / (% of p24+ cells in Targets) by gating on infected lived target cells.

ELISA

The gp120 inner domain stabilized ID2 (Tolbert et al., 2016) (0.1μg/ml) was diluted in PBS. Bovine serum albumin (BSA) (0.1μg/ml) was used a negative control. Proteins were adsorbed to plates (MaxiSorp; Nunc) overnight at 4°C. Coated wells were subsequently blocked with blocking buffer (tris-buffered saline (TBS) containing 0.1% Tween-20 and 2% (w/v) BSA for 1:30 hour at room temperature. HIV+ sera (1:1000 dilution) were diluted in blocking buffer and added to the coated wells for 1:30 hour at room temperature. Wells were washed four times with washing buffer (TBS containing 0.1% Tween-20). Horseradish peroxidase-conjugated (HRP) antibody specific of human IgG (Pierce) was added for 1 hour at room temperature, followed by four washes. HRP enzyme activity was determined after the addition of a 1:1 mix of Western Lightning oxidizing and luminol reagents (Perkin Elmer Life Sciences). Light emission was measured with the LB 941 TriStar luminometer (Berthold Technologies).

Cryo-EM Grid Preparation

Freshly thawed Aldrithiol-2 (AT-2)-inactivated HIV-1 particles (Lot#P4311, final concentration 335μg/mL in TNE buffer based on capsid protein concentration) were mixed with the CD4mc BNM-III-170 (5μM) and two anti-HIV-1 antibodies, 17b (5μg/mL) and A32 (5μg/mL). The mixture was pre-incubated at 37°C for 30 min prior to EM grid preparation. Two μL of this mixture was dispensed on glow-discharged Quantifoil R2/2 grids before plunge freezing in liquid ethane cooled by liquid nitrogen using Vitrobot (FEI-MarkIV). A total of 1033 movies was collected using a K2 camera mounted on a Talos Arctica transmission electron microscope placed in the Melbourne Advanced Microscopy Facility (MAMF) at the Bio21 Institute. In-situ single particle reconstruction was performed using the Scipion suite is described in Figure S4 (de la Rosa-Trevín et al., 2016).

Structural Model Building

Model building in the final cryo-EM density was performed by manually docking the crystal structure of the 17b antibody-bound HIV-1 $(gp41/gp120)_3$ hetero-trimer (PDB: 5VN3) in UCSF Chimera (Pettersen et al., 2004). The initial placement of the model was followed by independent rigid docking of each gp41/gp120 hetero-dimer into the segmented Cryo-EM density using the SeggeR tool (Pintilie et al., 2010) in UCSF Chimera. The position of each gp41-gp120 heterodimer was fine tuned in light of the segmented cryo-EM map produced by SeggeR and prior knowledge of epitope binding positions of the 17b and A32 antibodies obtained from crystal structures, 5VN3 (for 17b epitope) and 4YBL (for A32 epitope), respectively.

QUANTIFICATION AND STATISTICAL ANALYSIS

Analysis of Flow Cytometry Data

Statistics were analyzed using GraphPad Prism version 6.01 (GraphPad). Every data set was tested for statistical normality and this information was used to apply the appropriate (parametric or nonparametric) statistical test. P values <0.05 were considered significant; significance values are indicated as * $p<0.05$, ** $p<0.01$, *** $p<0.001$, **** $p<0.0001$.

Analysis of smFRET Data

The smFRET traces were processed and analyzed using the SPARTAN software package in Matlab (Mathworks) (Juette et al., 2016). The number of individual molecules analyzed in each experiment in indicated on the population FRET histograms (N). The number of distinct states present in the smFRET trajectories was quantitatively determined by fitting the traces to 3- and 4-state models using the Baum-Welch algorithm. The maximized likelihood determined during fitting was adjusted for the different numbers of model parameters using the Akaike Information Criterium (AIC), where AIC = 2k-2*L*, *k* is the number of model parameters (12 for the 3-state model; 20 for the 4-state model), and *L* is the maximum likelihood. Reduction in the AIC indicates improved model fitness. See Figure S3 for further details on HMM analysis.

DATA AND SOFTWARE AVAILABILITY

The structural model of $HIV\text{-}1_{BaL}$ Env bound to BNM-III-170, 17b, and A32 has been deposited into the EM Data Bank with accession number EMD-0466.